http://doi.org/10.35784/iapgos.6340 *received: 25.06.2024 | revised: 02.12.2024 | accepted: 16.12.2024 | available online: 21.12.2024*

POLARIZATION SELECTOR ON WAVEGUIDES PARTIALLY FILLED BY DIELECTRIC

Vitaly Pochernyaev[1], Nataliia Syvkova[1], Mariia Mahomedova[2]
[1]National Academy of Security Service of Ukraine, Kyiv, Ukraine, [2]Kyiv Professional College of Communications, Kyiv, Ukraine

Abstract. *In this article, a polarization selector, which based on waveguides partially filled by dielectric has been developed and investigated. An analysis of the designs of polarization selectors on empty waveguides was carried out. The developed design of the polarization selector is based on square waveguides partially filled by dielectric in the form of an E-tee. The main and side waveguides of the E-tee include metal gratings with mutually perpendicular conductors. The dielectric plates have a square cross-section and extend between the second and third conductors of metal grids, which located in the main and side waveguides. The article presents the normalized conductivity for such an E-tee, through which the standing wave coefficient is determined. The normalized conductivity of the E-tee consists of the reactive conductivity of the joint of the side square waveguide partially filled by dielectric, the reactive conductivity of the joint of the main square waveguide partially filled by dielectric, reactive conductivity of grids in side and main waveguide partially filled by dielectric. These conductivities are determined through the corresponding transformation coefficients, which are combinations of selected coordinate functions and the electrical transverse and magnetic transverse eigenvector functions of a waveguide partially filled by dielectric. The transverse electric and transverse magnetic eigenvector functions of a waveguide partially filled by dielectric are expressed through the Mathieu functions and their derivatives. Numerical results were obtained for the reactive conductivities of gratings from the ratio of the thickness of the grating rod to the size of the wall of a square waveguide for different normalized wavelengths. The results were obtained both for a grid with equal distances between the rods and for unequal spaced rods.*

Keywords: polarization selector, waveguide partially filled by dielectric, standing wave coefficient, transverse electric eigenvector function, transverse magnetic eigenvector function

SELEKTOR POLARYZACJI NA FALOWODACH CZĘŚCIOWO WYPEŁNIONYCH DIELEKTRYKIEM

Streszczenie. *W niniejszym artykule opracowano i zbadano selektor polaryzacji oparty na falowodach częściowo wypełnionych dielektrykiem. Przeprowadzono analizę konstrukcji selektorów polaryzacji na pustych falowodach. Opracowany projekt selektora polaryzacji oparty jest na kwadratowych falowodach częściowo wypełnionych dielektrykiem w postaci E-trójnika. Główny i boczne falowody E-trójnika zawierają metalowe kraty z wzajemnie prostopadłymi przewodnikami. Płytki dielektryczne mają kwadratowy przekrój poprzeczny i rozciągają się między drugim i trzecim przewodnikiem metalowych siatek, które znajdują się w głównym i bocznych falowodach. W artykule przedstawiono znormalizowaną przewodność dla takiej płytki E-trójnika, za pomocą której określa się współczynnik fali stojącej. Znormalizowana przewodność E-trójnika składa się z przewodności biernej złącza bocznego falowodu kwadratowego częściowo wypełnionego dielektrykiem, przewodności biernej złącza głównego falowodu kwadratowego częściowo wypełnionego dielektrykiem, przewodności biernej siatek w falowodzie bocznym i głównym częściowo wypełnionych dielektrykiem. Przewodności te są określane za pomocą odpowiednich współczynników transformacji, które są kombinacjami wybranych funkcji współrzędnych oraz elektrycznych poprzecznych i magnetycznych poprzecznych funkcji wektora własnego falowodu częściowo wypełnionego dielektrykiem. Poprzeczne elektryczne i poprzeczne magnetyczne funkcje wektora własnego falowodu częściowo wypełnionego dielektrykiem są wyrażone za pomocą funkcji Mathieu i ich pochodnych. Uzyskano wyniki numeryczne dla przewodności biernej siatek na podstawie stosunku grubości pręta siatki do rozmiaru ściany kwadratowego falowodu dla różnych znormalizowanych długości fal. Wyniki uzyskano zarówno dla siatki o równych odległościach między prętami, jak i dla prętów o nierównych odstępach.*

Słowa kluczowe: selektor polaryzacji, falowód częściowo wypełniony dielektrykiem, współczynnik fali stojącej, poprzeczna elektryczna funkcja wektora własnego, poprzeczna magnetyczna funkcja wektora własnego

Introduction

The antenna-feeder paths of mobile digital troposcatter communication stations and troposcatter components of combined mobile digital troposcatter-radiorelay [9] and mobile digital troposcatter-space [10] stations contain polarization selectors. These devices are designed to separate transmitted and received signals with electromagnetic field polarization planes that differ by $\pi/2$. In some cases, as is done in the above communication stations, signals are transmitted with either vertical or horizontal polarization, and signals are received with both polarizations. Then in the receiving part of the antenna-feeder path there should be a polarization selector that separates the vertical and horizontal polarization into two receiving microwave paths. However, the antenna-feeder paths of mobile combined communication stations are implemented on waveguides partially filled by dielectric (WPFD). Therefore, the task arises of developing a polarization selector based on the WPFD.

1. Analysis of the literature

An analysis of the literature shows that the main waveguide structures of polarization selectors consist of a circular or square axial waveguide and a rectangular single-mode waveguide located at an angle of $\pi/2$ to the axial waveguide. A longitudinal conductive plate is installed in an axial waveguide of circular cross-section. This plate allows evidence of one linear polarization to pass through and reflects a wave with another linear polarization into a side rectangular waveguide. The designs of polarization selectors that are most widely used are shown in reference books [2, 6]. Also, modifications of these designs were studied in [3, 5, 8, 12, 23], and polarization filtering in antennas of different types and different ranges was analysed in [1, 4, 7, 13–22, 24].

However, these traditional hollow waveguide designs have large transverse dimensions and sometimes require matching junctions. The developed design based on the WPFD is devoid of these disadvantages and can be used in waveguide phased antenna arrays, matrices of mirror antenna feeds, and axisymmetric antenna feeds to reduce mirror dimming.

The purpose of the article is to develop and study a polarization selector at WPFD.

2. Main part

Figure 1 shows a general view of the developed polarization selector, which based on square WPFD. This polarization selector consists of an *E*-tee made up of square WPFD and two metal grids with mutually perpendicular conductors. Dielectric plates of square cross-section are arranged to extend between the second and third grid conductors in the main and side waveguides. Fig. 1 shows the connection of the antenna (Ant) and two microwave receiving arms Rec1 and Rec 2. A wave with vertical polarization of vector $\overline{E}$ enters the arm of Rec 1, since it freely passes through an inclined grid with horizontal conductors in the main waveguide and is completely reflected from the grid in the side waveguide. A wave with horizontal polarization of vector $\overline{E}$ enters the Rec 2 arm, since it is reflected, like a mirror, by an inclined grid with horizontal conductors in the main waveguide and is directed into the side waveguide. The grid in this waveguide is perpendicular to the vector $\overline{E}$ and transmits such a wave.

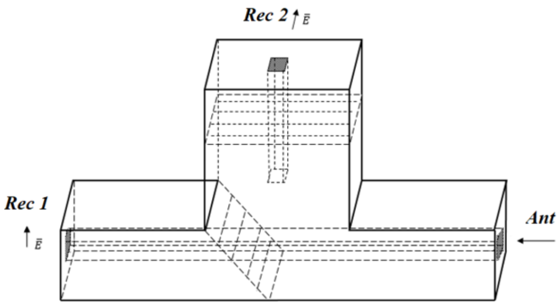

Fig. 1. Design of a polarization selector based on square WPFD

The operation of the device is based on the *E*-tee circuit. When an electromagnetic wave falls from the *E*-arm of the tee, the electric fields in the side arms of the main waveguide at equal distances from the joint are in antiphase. Magnetic fields at equal distances from the joint are in phase.

A square waveguide has an advantage over a round waveguide, since there are no critical frequencies of higher wave types in the required operating range. In the square WPFD, the operating mode is selected between the critical frequencies of the main waves quasi-H_{10} and quasi-H_{01} and the first higher types of waves quasi-H_{20} and quasi-H_{02}. This single-mode mode was chosen for practical reasons of durability of the waveguide, and, in general, of the entire device to increase the operating frequency band. In an hollow square waveguide, it is preferable to choose a multimode operating mode between the critical frequencies of the higher types of waves, quasi-H_{20} and quasi-H_{02}, and the critical frequencies of the higher types of waves, H_{11} and E_{11}.

The main parameter of the polarization selector is the standing wave coefficient (SWC) or traveling wave coefficient (TWC). The values of SWC and TWC are determined through the module of the reflection coefficient $|S_{11}|$:

$$SWC = \frac{1+|S_{11}|}{1-|S_{11}|} \qquad TWC = \frac{1-|S_{11}|}{1+|S_{11}|} \tag{1}$$

The equivalent circuit of the device in Fig. 1 is shown in Fig. 2.

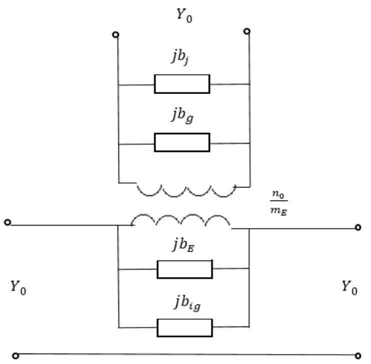

Fig. 2. Equivalent circuit of a polarization selector based on square WPFD

The diagram shows: Y_0 – the characteristic conductivity of a square WPFD [11]; jb_j – reactive conductivity of the joint from the side of the square WPFD; jb_E – reactive conductivity of the joint from the side of the main square WPFD; jb_g – reactive conductivity of the grid in the side square WPFD; jb_{ig} – reactive conductivity of the inclined grid in the main square WPFD.

The normalized conductivity of an *E*-tee with grid diaphragms is written in the form:

$$y = \left(\frac{n_0}{m_E}\right)\left(jb_j + jb_g\right) + jb_E + jb_{ig} \tag{2}$$

where n_0 – transformation coefficient for the fundamental wave of the square WPFD; m_E – *E*-tee transformation coefficient.

Since the characteristic conductance Y_0 in all arms of the *E*-tee are the same, the expression for $|S_{11}|$ is as follows:

$$|S_{11}| = \frac{y}{2+y} \tag{3}$$

Due to the cumbersomeness of the expression for the values of jb_E and m_E, we will not indicate them, but we will present these values graphically (Fig. 3), where curve 1 corresponds to the value of m_E, and curve 2 – to the value of b_E.

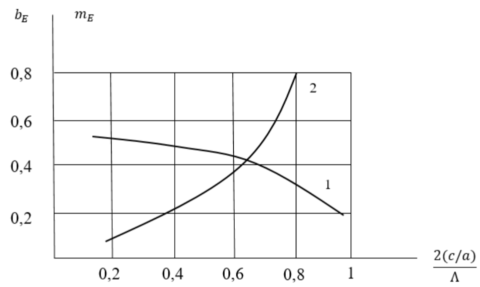

Fig. 3. Dependence of the reactive conductivity b_E and the module of the transformation ratio m_E on the normalized wavelength

The expression for the reactance of the junction jb_j is as follows:

$$b_j = (1/n_0)^2 \sum_{k=1}^{\infty} n_k^2 y_k \tag{4}$$

where n_k – transformation coefficient for higher of types waves of square WPFD; y_k – normalized conductivities of higher wave types [11].

Necessary expressions for determining the transformation coefficients in formula (4):

$$n_0 = \int_S \bar{\varepsilon}_{h10} \bar{\varepsilon}_{h01} dS \tag{5}$$

$$n_k = \int_S \bar{Э}_k \sum_{k=1} \bar{\varepsilon}_k dS \tag{6}$$

where $\bar{\varepsilon}_{h10}, \bar{\varepsilon}_{h01}$ – transverse electrical eigenvector functions of quasi-H_{10} and quasi-H_{01} waves; $\bar{\varepsilon}_k$ – transverse electrical eigenvector functions of high wave types; $\bar{Э}_k$ – coordinate function; *S* – cross section of a square waveguide.

We take the coordinate function $\bar{Э}_k$ in expression (6) in the form:

$$\bar{Э}_k = \bar{\varepsilon}_{h10} + \bar{\varepsilon}_{h01} + \bar{\varepsilon}_{h30} \tag{7}$$

where $\bar{\varepsilon}_{h10} + \bar{\varepsilon}_{h01} + \bar{\varepsilon}_{h30}$ – transverse electrical eigenvector functions quasi-H_{10}, quasi-H_{01}, quasi-H_{30}.

The correction factor for formulas (5) is as follows:

$$k_c = \frac{3\pi^2 b}{a} - \frac{b}{128\,a}(3q\pi)^2 + \frac{a}{8\,b}[(p\pi)^2 + (qp\pi)^2] \tag{8}$$

The correction factor according to formula (8) increases the accuracy of formula (5) by 3%.

As a first approximation for $k = 3$, we take the eigenvector functions of the quasi-H_{10}, quasi-H_{20}, quasi-H_{01} waves as the function $\bar{\varepsilon}_k$.

Taking into account the transverse electrical eigenvector functions of quasi-H_{11} and quasi-E_{11} waves increases the accuracy of the calculation using formula (6) by 1.5%. This is explained by the correct choice of the coordinate function $\bar{Э}_k$, defined by formula (7).

We will calculate the values of jb_g and jb_{ig} as follows.

As coordinate functions $\bar{Э}_j$ and $\bar{Э}_{ig}$, approximating the field on the grids, we take the sum of the transverse electric and transverse magnetic eigenvector functions of the quasi-H_{10} and quasi-H_{30} waves:

$$\bar{Э}_j = \bar{\varepsilon}_{h10} + \bar{\mathcal{H}}_{h10} + \bar{\varepsilon}_{h30} + \bar{\mathcal{H}}_{h30}$$
$$\bar{Э}_{ig} = (1/\sin\phi)[\bar{\varepsilon}_{h10} + \bar{\mathcal{H}}_{h10} + \bar{\varepsilon}_{h30} + \bar{\mathcal{H}}_{h30}] \qquad (9)$$

where $\bar{\varepsilon}_{h10}, \bar{\varepsilon}_{h30}$ – transverse electric eigenvector functions of waves; $\bar{\mathcal{H}}_{h10}, \bar{\mathcal{H}}_{h30}$ – transverse magnetic eigenvector functions of quasi-H_{10} and quasi-H_{30} waves; ϕ – angle of inclination of the grid's diaphragm $\frac{\pi}{4} \le \phi \le \frac{\pi}{2}$.

If the eigenvector functions are written in terms of Mathieu functions, then they look like this:

$$\bar{\varepsilon}_{h10} = \left(\sqrt{128/ab(64+q^2+p^2+q^2p^2} \,/\, \chi_{h10}\right)$$
$$[Ce_1(q,\xi)Ce_0^{/}(p,\eta)\bar{\xi}^0 - Ce_1^{/}(q,\xi)Ce_0(p,\eta)\bar{\eta}^0]$$
$$\bar{\varepsilon}_{h30} = \left(\sqrt{128/ab(64+q^2+p^2+q^2p^2} \,/\, \chi_{h30}\right)$$
$$[Ce_3(q,\xi)Ce_0^{/}(p,\eta)\bar{\xi}^0 - Ce_3^{/}(q,\xi)Ce_0(p,\eta)\bar{\eta}^0] \qquad (10)$$
$$\bar{\mathcal{H}}_{h10} = \left(\sqrt{128/ab(64+q^2+p^2+q^2p^2} \,/\, \chi_{h10}\right)$$
$$[Ce_1^{/}(q,\xi)Ce_0(p,\eta)\bar{\xi}^0 + Ce_1(q,\xi)Ce_0^{/}(p,\eta)\bar{\eta}^0]$$
$$\bar{\mathcal{H}}_{h30} = \left(\sqrt{128/ab(64+q^2+p^2+q^2p^2} \,/\, \chi_{h30}\right)$$
$$[Ce_3^{/}(q,\xi)Ce_0(p,\eta)\bar{\xi}^0 + Ce_3(q,\xi)Ce_0^{/}(p,\eta)\bar{\eta}^0]$$

where

$Ce_1(q,\xi), Ce_0(q,\xi), Ce_3(q,\xi), Ce_1(p,\eta), Ce_0(p,\eta)$ – even Mathieu functions; $Ce_1^{/}(q,\xi), Ce_0^{/}(q,\xi), Ce_3^{/}(q,\xi), Ce_1^{/}(p,\eta), Ce_0^{/}(p,\eta)$ – derivatives of even Mathieu functions.

Expression (9) is found using formulas (10).

In our case, for a grid of four thin rods, we take waves of type H_{m0} with index m equal to m = 9, 11, 19, 21, 29, … as local fields. For example, for a two-rod grid, the index m = 5, 7, 11, 13, 17, 19, 23, … Here it is enough to limit ourselves to the quasi-$H_{9\,0}$ and quasi-$H_{11\,0}$ waves to find the reactive conductivities jb_j and jb_{ig}. Their eigenvector functions are written as follows:

$$\bar{\varepsilon}_{h9\,0} = \left(\sqrt{128/ab(64+q^2+p^2+q^2p^2} \,/\, \chi_{h9\,0}\right)$$
$$[Ce_9(q,\xi)Ce_0^{/}(p,\eta)\bar{\xi}^0 - Ce_9^{/}(q,\xi)Ce_0(p,\eta)\bar{\eta}^0]$$
$$\bar{\mathcal{H}}_{h9\,0} = \left(\sqrt{128/ab(64+q^2+p^2+q^2p^2} \,/\, \chi_{h9\,0}\right)$$
$$[Ce_9^{/}(q,\xi)Ce_0(p,\eta)\bar{\xi}^0 + Ce_9(q,\xi)Ce_0^{/}(p,\eta)\bar{\eta}^0] \qquad (11)$$
$$\bar{\varepsilon}_{h11\,0} = \left(\sqrt{128/ab(64+q^2+p^2+q^2p^2} \,/\, \chi_{h11\,0}\right)$$
$$[Ce_{11}(q,\xi)Ce_0^{/}(p,\eta)\bar{\xi}^0 - Ce_{11}^{/}(q,\xi)Ce_0(p,\eta)\bar{\eta}^0]$$
$$\bar{\mathcal{H}}_{h11\,0} = \left(\sqrt{128/ab(64+q^2+p^2+q^2p^2} \,/\, \chi_{h11\,0}\right)$$
$$[Ce_{11}^{/}(q,\xi)Ce_0(p,\eta)\bar{\xi}^0 + Ce_{11}(q,\xi)Ce_0^{/}(p,\eta)\bar{\eta}^0]$$

where:

$Ce_0(p,\eta), Ce_9(q,\xi), Ce_{11}(q,\xi)$ – even Mathieu functions of zero, 9 and 11 orders;

$Ce_0^{/}(p,\eta), Ce_9^{/}(q,\xi), Ce_{11}^{/}(q,\xi)$ – derivatives of even Mathieu functions of zero, 9 and 11 orders.

Table. 1. Reactive conductivities of the 4 – rods grid diaphragms

a/λ	Grid in the side waveguide	Incline grid in the main waveguide
	b_j	b_{ig}
0,72	10	14
0,76	11	16
0,8	13	19

Calculation of the conductivity of the grid diaphragm at $a/\lambda = 0.7$ in the side section of the waveguide tee (polarization selector) is shown in Fig. 4.

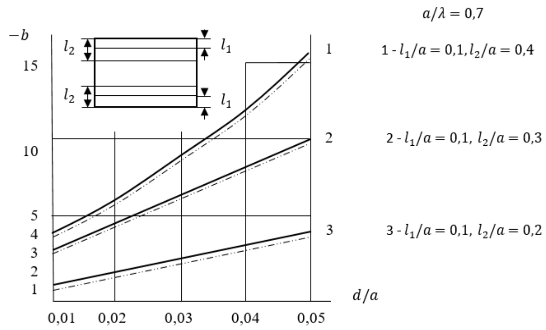

Fig. 4. Dependence of the reactive conductivity of the grid diaphragms in the side waveguide of the d/a ratio (unequal distances between the rods)

Solid curves are graphs, which constructed using basic formulas. The dotted curves are graphs, which constructed using formulas with a correction factor. Curve 1 corresponds to the value $l_1/a = 0.1; l_2/a = 0.4$. Curve 2 corresponds to the value $l_1/a = 0.1; l_2/a = 0.3$. Curve 3 corresponds to the value $l_1/a = 0.1; l_2/a = 0.2$. The unequal distances between the rods were chosen for the convenience of locating a dielectric plate with a square cross-section if it were necessary to increase the size of this cross-section.

Fig. 5 shows the dependence of the reactive conductivity of a four-rod grating diaphragm with equal distances between the rods $a/5$ located in the side waveguide as a function of d/a. The ratio $a/\lambda = 0.7$ corresponds to the lower limit of the frequency range of the digital troposcatter station, the ratio $a/\lambda = 0.75$ corresponds to the middle of the frequency range of the digital troposcatter station, the ratio $a/\lambda = 0.8$ corresponds to the upper limit of the frequency range of the digital troposcatter station. The graphs show that as the operating frequency increases, the reactive conductivity of the diaphragm decreases.

All quantities in formula (2) are determined through formulas (4)–(11) and graphs in Fig. 3. Substituting expression (2) into expression (3), and the modulus of expression (3) into expression (1), we find SWC or TWC.

Resulting of Fig. 4 and Fig. 5 are used by formulas (10), (11).

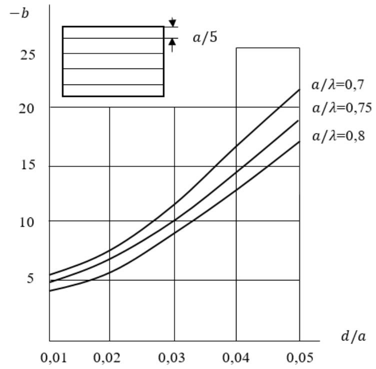

Fig. 5. Dependences of the reactive conductivity of the grid diaphragms in the side waveguide on the d/a ratio (equal distances between the rods)

3. Conclusions

A polarization selector based on square WPFD can be classified as a broadband device with an operating frequency band of ~45%. The SWC value is no worse than 1.12. At the junction of the square WPFD, quasi-H_{01} and quasi-H_{30} waves are taken into account, at the diaphragm, quasi-H_{90} and quasi-$H_{11\ 0}$ waves.

For researchers of similar devices the data in Fig. 4 and Fig. 5 are useful. These data are related to questions of placement and dimensions of the dielectric rod, which were investigated in the monograph [11].

A polarization selector based on square WPFD can be used in digital troposcatter stations, waveguide phased array antennas and reflector antenna feed matrices. The main positions of theory of the WPFD is developed in transactions [11]. As the a/λ ratio increases, the reactive conductivity of the grid diaphragms will decrease. As the number of grid diaphragms increases, the number of higher types of waves taken into account will decrease while achieving the same calculation accuracy.

References

[1] Cheng G. et al.: A Stacked Circularly Polarized Filtering Antenna With Crossed Slot. IEEE Antennas and Wireless Propagation Letters. 2023, 22(12), 2935–2939.

[2] Handbook: Digital Radio-Relay Systems. ITU Radiocommunication Bureau, Geneva, 1996.

[3] He Y. et al.: Dual-Polarized Filtering Antenna Array for 5G Base Station Applications. International Conference on Microwave and Millimeter Wave Technology (ICMMT). China, Harbin, 2022, 1–3 [https://doi.org/10.1109/ICMMT55580.2022.10022492].

[4] Huang K. et al.: Dual-Polarized Filtering Antenna Based on a Second-Order SIR Filter. IEEE Antennas and Wireless Propagation Letters 23(1), 2024, 154–158.

[5] Jia Q., Ding S., Zhu Z., Wang B.: A Multifunctional Broadband Linear-Circular Polarization Conversion Transmission Metasurface. International Conference on Microwave and Millimeter Wave Technology (ICMMT). China, Qingdao, 2023, 1–3 [https://doi.org/10.1109/ICMMT58241.2023.10277184].

[6] Kantor L. Ya. (red.): Sputnykovaya svyaz' y veshchanye: Spravochnyk. Radyo y svyaz. Moscow 1988.

[7] Li H.-M. et al.: Compact Broadband Filtering Differential Dielectric Resonator Antenna for Dual-Polarized Applications. IEEE Antennas and Wireless Propagation Letters 23(1), 2024, 384–388 [https://doi.org/10.1109/LAWP.2023.3325411].

[8] Nickel M. et al.: A liquid crystal based tunable polarization selector in a microwave imaging radiometer. 11th German Microwave Conference (GeMiC). Germany, Freiburg, 2018, 91–94 [https://doi.org/10.23919/GEMIC.2018.8335036].

[9] Pochernyaev V. M., Povkhlib V. S.: Mobil'na tsyfrova troposferno-radioreleyna stantsiya. Ukrainian Patents Database. Patent number: 112217 C2. app. 12.09.2014, publ. 10.08.2016 [https://ua.patents.su/10-112217-mobilna-cifrova-troposferno-radiorelejjna-stanciya.html].

[10] Pochernyaev V. M., Povkhlib V. S.: Mobil'na tsyfrova troposferno-radioreleyna stantsiya. Ukrainian Patents Database. Patent number: 126203 C2. app. 17.01.2020, publ. 10.08.2020.

[11] Pochernyaev V. M., Tsybizov K. M.: Teoriya skladnykh khvylevodiv. Naukovyy svit, 2003.

[12] Skovorodnikov S. V., Sinyaev Y. A.: Application of Higher-order Wave Modes Filter for Measurement of Phased Antenna Array Elements. Antennas Design and Measurement International Conference (ADMInC). Russian Federation, Saint Petersburg, 2021, 61–63 [https://doi.org/10.1109/ADMInC54110.2021.9671007].

[13] Song X., Wu X., Hu Y.: Planar circularly polarization filter antenna design for the 2.4GHz Bluetooth band. International Applied Computational Electromagnetics Society Symposium (ACES-China). China, Xuzhou, 2022, 1–4 [https://doi.org/10.1109/ACES-China56081.2022.10064915].

[14] Wang J. et al.: A Wideband Circularly Polarized Filtering Antenna Based on Slot-Patch Structure. IEEE Antennas and Wireless Propagation Letters 22(8), 2023, 1858–1862.

[15] Wang W. et al.: Circularly Polarized Patch Antenna With Filtering Performance Using Polarization Isolation and Dispersive Delay Line. IEEE Antennas and Wireless Propagation Letters 19(8), 2020, 1457– 1461.

[16] Xu T. et al.: A Wideband Circularly Polarized Filtering Patch Antenna With Strip Network. IEEE Antennas and Wireless Propagation Letters 22(12), 2023, 2826–2830.

[17] Yang S. J., Zhang X. Y.: Millimeter-Wave Dual-Polarized Filtering Antenna Design for 5G AiP Application. IEEE MTT-S International Microwave Filter Workshop (IMFW). Italy, Perugia, 2021, 159–161 [https://doi.org/10.1109/IMFW49589.2021.9642335].

[18] Yuan H., Chen F.-C., Chu Q.-X.: A Wideband and High Gain Dual-Polarized Filtering Antenna Based on Multiple Patches. IEEE Transactions on Antennas and Propagation 70(10), 2022, 9843–9848 [https://doi.org/10.1109/TAP.2022.3177494].

[19] Zhai J. H., Jing Xiao Z., Cao Y. F.: Millimeter-Wave Wideband Circularly Polarized Filtering Antenna for Satellite Communication. 16th UK-Europe-China Workshop on Millimetre Waves and Terahertz Technologies (UCMMT). China, Guangzhou, 2023, 1–3 [https://doi.org/10.1109/UCMMT58116.2023.10310621].

[20] Zhang P.-P. et al.: Design of Single-Layer Circularly Polarized Filtering Reflectarray Antenna. IEEE MTT-S International Wireless Symposium (IWS). China, Qingdao, 2023, 1–3 [https://doi.org/10.1109/IWS58240.2023.10222869].

[21] Zhao W. et al.: A Millimeter-Wave Dual-Polarized Filtering Patch Antenna Array Supported by High-Order SIW Cavity. IEEE 5th International Conference on Electronic Information and Communication Technology (ICEICT). China, Hefei, 2022, 412–414 [https://doi.org/10.1109/ICEICT55736.2022.9909079].

[22] Zheng Y. Y. et al.: A Compact Full-metal Circularly Polarized Filtering Antenna with an Embedded Metasurface. IEEE MTT-S International Microwave Workshop Series on Advanced Materials and Processes for RF and THz Applications (IMWS-AMP). China, Guangzhou, 2022, 1–2 [https://doi.org/10.1109/IMWS-AMP54652.2022.10106855].

[23] Zhong X. et al.: Circularly Polarized Filtering Antenna Based on Integrated Substrate Gap Waveguide. IEEE MTT-S International Wireless Symposium (IWS). China, Nanjing, 2021, 1–3 [https://doi.org/10.1109/IWS52775.2021.9499709].

[24] Zhou J. et al.: A Wideband Circularly Polarized Filtering Antenna Based on Stacked Patch Structure. IEEE MTT-S International Microwave Workshop Series on Advanced Materials and Processes for RF and THz Applications (IMWS-AMP). China, Chengdu, 2023, 1–3 [https://doi.org/10.1109/IMWS-AMP57814.2023.10381421].

Prof. Vitaly Pochernyaev
e-mail: vpochernyaev@gmail.com

Doctor of Technical Sciences, professor, member of the Institute of Electrical and Electronics Engineers, professor at the National Academy of Security Service of Ukraine. Author of more than 200 publications, including 3 monographs, 2 textbooks, 12 patents for inventions.
Research interests: applied electrodynamics, radiophysics, telecommunications and radio-engineering, microwave theory and technology.

http://orcid.org/0000-0001-7130-8668

Ph.D. Nataliia Syvkova
e-mail: natsivonat@gmail.com

Doctor of Philosophy, docent National Academy of Security Service of Ukraine. Author of more than 40 publications, including 1 textbook and 5 patents for inventions.
Research interests: telecommunications and radio-engineering, microwave theory and technology.

http://orcid.org/0000-0002-4934-4109

Ph.D. Mariia Mahomedova
e-mail: kkz.praktika@ukr.net

Doctor of Philosophy, lecturer at the Kyiv Professional College of Communications. Author of more than 28 publications, including 1 patents for inventions.
Research interests: telecommunications and radio-engineering, microwave theory and technology.

http://orcid.org/0000-0003-1936-5555